SUbsonic Single Aft eNgine (SUSAN) Power/Propulsion System Control Architecture Updates

Jonah. J. Sachs-Wetstone[1], Jonathan S. Litt[2], Jonathan L. Kratz[3], and Halle E. Buescher[4]

NASA Glenn Research Center, Cleveland, OH, 44135, USA

The development of hybrid-electric propulsion technology for commercial transport aircraft presents opportunities for new designs that can reduce fuel consumption and greenhouse gas emissions and improve safety and reliability compared to modern aircraft. The SUbsonic Single Aft eNgine (SUSAN) Electrofan is a conceptual design for a transport aircraft with a series/parallel partial hybrid-electric propulsion system that is being developed by NASA as a reference design for a regional transport aircraft with a high degree of electrification. The SUSAN concept incorporates multiple tightly coupled power, propulsion, and flight control systems that introduce new challenges to the control design process, requiring a hierarchical and more coordinated control approach. This paper summarizes updates to the SUSAN Power/Propulsion System (PPS) model and control architecture made in preparation for planned flight simulator and hardware-in-the-loop testing at NASA Glenn Research Center. These updates include a new electrical power system model developed using the NASA-developed Electrical Modeling and Thermal Analysis Toolbox (EMTAT) and a new PPS control architecture that improves the operational flexibility and responsiveness of the propulsion system. The performance of the updated controller is demonstrated and discussed.

I. Nomenclature

Alt	=	altitude above sea level in standard atmosphere, ft
C	=	capacitance, farads
dTamb	=	temperature difference from standard day, °R
e(t)	=	state error
F_{net}	=	net thrust, lbf
K_i	=	integral gain
K_p	=	proportional gain
K_{iwp}	=	integral windup protection gain
MN	=	Mach number
N_1	=	geared turbofan fan speed, rpm
N_2	=	geared turbofan low-pressure shaft speed, rpm
N_3	=	geared turbofan high-pressure shaft speed, rpm
N_{WF}	=	electric engine wingfan shaft speed, rpm
N_c	=	corrected shaft speed, rpm
P_2	=	total pressure at station 2 (fan inlet), psi
P_{25}	=	total pressure at station 25 (low-pressure compressor inlet), psi

[1] Aerospace Engineer, Intelligent Control and Autonomy Branch, AIAA Member.
[2] Aerospace Engineer, Intelligent Control and Autonomy Branch, AIAA Associate Fellow.
[3] Aerospace Engineer, Intelligent Control and Autonomy Branch, AIAA Senior Member.
[4] Mechanical Engineer, Intelligent Control and Autonomy Branch, AIAA Member.

P_3 = total pressure at station 3 (high-pressure compressor discharge), psi
Ps_3 = static pressure at station 3 (high-pressure compressor discharge), psi
R = resistance, ohms
SoC = battery State of Charge, %
SP = setpoint
T_3 = total temperature at station 3 (HPC discharge), °R
T_4 = total temperature at station 4 (HPT inlet), °R
$u(t)$ = nominal control output
$u^*(t)$ = actual control output
W = mass flow rate, lbm/s
W_f = fuel flow rate, lbm/s
τ = RC circuit time constant, s

II. Introduction

The commercial aviation sector is both a significant contributor to the causes of climate change and a victim of its effects [1, 2, 3], and it is therefore of critical importance that the aviation industry work to reduce its negative impacts on the global climate. However, mitigating the negative environmental impacts of transport class aircraft presents a unique set of challenges, requiring technological leaps as well as infrastructure and operational changes to overcome. Research efforts in this area have led to electrified aircraft propulsion (EAP) technologies becoming a major focus for the aviation community. The National Aeronautics and Space Administration's (NASA) Aeronautics Research Mission Directorate (ARMD) has been working with other government agencies as well as partners in industry and academia to understand and develop EAP technologies for future aircraft [4, 5, 6, 7]. There has been significant progress made in recent years on the development of novel short-haul, all-electric vehicles [8], but significant technology barriers remain before all-electric transport-class aircraft can be considered a feasible alternative to hydrocarbon powered vehicles [9, 10]. Hybrid-electric aircraft propulsion technology offers an intermediate step on the road to zero carbon emissions, potentially providing significant improvements in fuel burn, emissions, noise, and safety [9] and significantly expanding the design space for new aircraft by enabling greater meshing airframe, and flight control, and mechanical/electrical propulsion systems. However, these aircraft also present unique challenges with respect to aircraft certification and safety [11, 12], subsystem integration, and control design [13, 14].

To address these challenges, the NASA Convergent Aeronautics Solutions (CAS) project has been developing the SUbsonic Single Aft eNgine (SUSAN) Electrofan concept aircraft [15] as an advanced hybrid-electric design with a 20 MW EAP system that incorporates propulsion airframe integration (PAI), boundary layer ingestion (BLI), and distributed electric propulsion (DEP) technologies to reduce fuel burn by up to 50% per passenger mile while retaining the capabilities of modern large regional jets. Concept renderings of the SUSAN vehicle are shown in Fig. 1. The SUSAN trade space is still being explored and the design is expected to evolve as trades are refined and additional studies are completed across a wide variety of disciplines at varying degrees of fidelity. The focus of this paper will be a set of updates to the dynamic SUSAN power/propulsion system (PPS) model and control design presented in [16, 17]. These updates were made to bring the existing model in line with recent trade space revisions and improve capabilities that leverage the hybrid-electric features of the powertrain, resulting in a dynamic, component based, full envelope PPS model and control system that is planned for use in several upcoming studies at the NASA Glenn Research Center (GRC). Results from these studies will be used to feed back into the ongoing SUSAN concept maturation, including the further development of the PPS.

As is common with EAP systems [14], the control design for the SUSAN power and propulsion systems presents unique challenges due to its complexity and the tightly coupled nature of the many different subsystems. In addition

Figure 1. NASA concept renderings of the SUSAN Electrofan aircraft.

to a hybridized turbofan engine the SUSAN Electrofan PPS has 16 distributed electric propulsors that it uses to produce normal thrust, provide augmented thrust for short periods, and implement DEP by allowing the magnitude of control surface deflections required for normal attitude control to be reduced. Controlling this complex system requires a control architecture capable of balancing multiple control priorities simultaneously.

The rest of this paper is organized as follows. First, a brief overview of the current full-scale SUSAN concept is given in Section III. A summary of the updates to the power and propulsion model is presented in Section IV, and the revised control architecture is presented in Section V. Results from the model illustrating the improved capabilities are shown in Section VI. Planned applications of the model are discussed in Section VII, followed by concluding remarks in Section VIII.

III. SUSAN Electrofan Concept

The SUSAN Electrofan is a concept design developed by the NASA CAS project as an advanced single-aisle transport class airliner designed to match the capabilities of modern large regional jets. The concept is comparable in payload, size, and range to a Boeing 737 MAX or an Airbus A320neo. It has a 750 nautical mile economic mission, a design range of 2500 nautical miles, and can carry up to 180 passengers. The design features large-scale turbofan electric power extraction supporting a 20 MW EAP system. Additional details and discussion on the SUSAN concept can be found in Refs. [15, 16, 17, 18]. The focus of this paper is a set of recent updates to the dynamic system level model of the PPS and the design of the control system. The SUSAN PPS (Fig. 2) consists of a single, aft-mounted

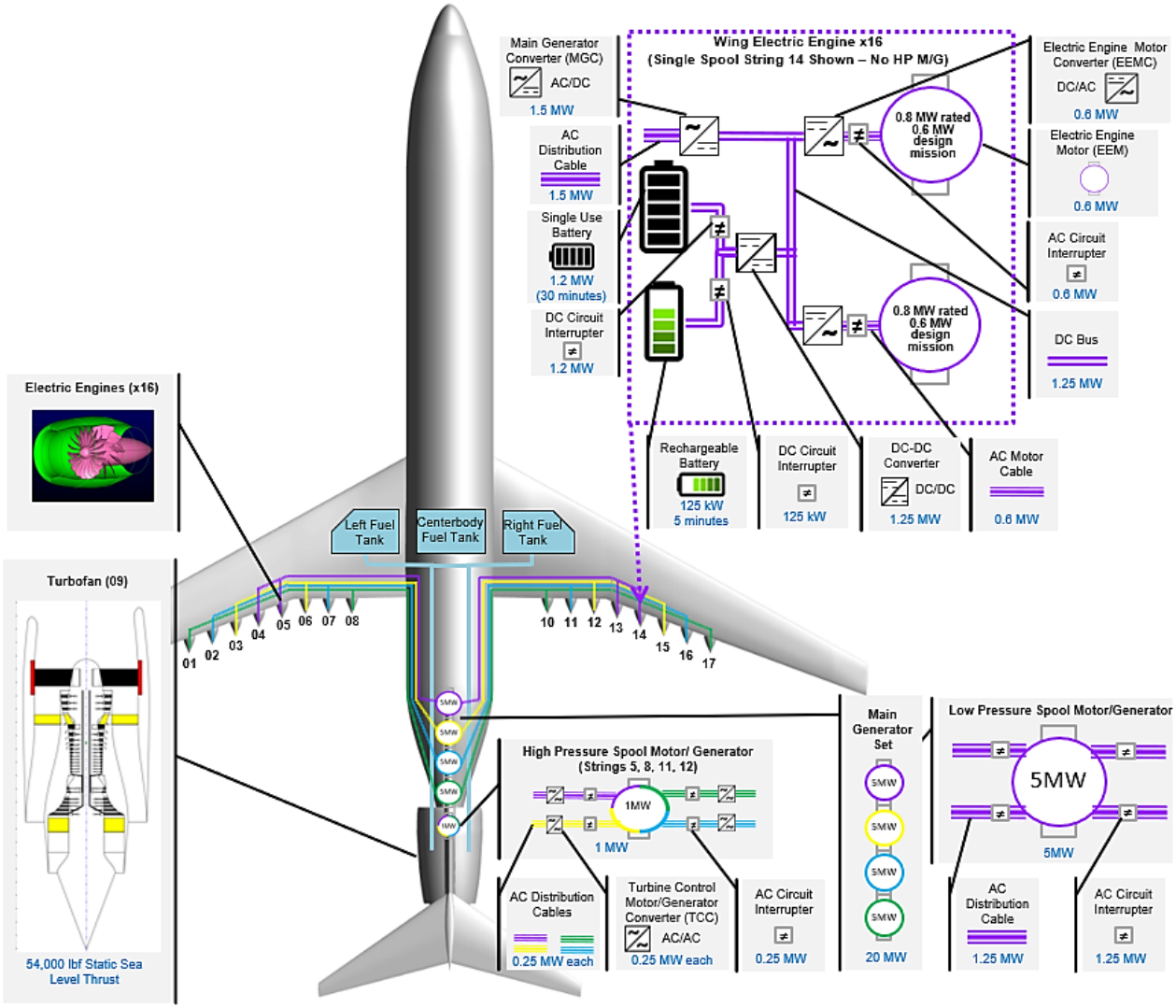

Figure 2. System diagram of the SUSAN Power/Propulsion subsystems, illustrating the arrangement of the 16 electric engine strings. A detail of the electrical system for one single-spool string (14) is shown upper right).

BLI geared turbofan engine (GTF) that both produces thrust and supplies mechanical offtake power to generators producing up to 20 MW of electrical power. The electrical power is sent to 16 electric engines (EEs) consisting of two arrays of eight two-stage contra-rotating BLI ducted fans with one array mounted under each wing in a mail-slot configuration. This configuration allows the propulsion system to augment the flight controls through DEP [19]. Each EE, also referred to as a wingfan, is driven by a pair of wound-field 3-phase synchronous motors. The turbomachinery is sized such that GTF produces approximately 1/3 of the total thrust across all phases of flight, with the remaining 2/3 thrust split evenly between the arrays of EEs on each wing [20]. The propulsors are numbered 01 through 17 from left to right, with 09 referring to the turbofan, in accordance with engine numbering conventions.

A simplified diagram of the SUSAN power and propulsion subsystems is shown in Fig. 2. To increase safety and reliability, the electrical power system (EPS) is designed for maximum redundancy. There are 16 wound-field motor/generator (M/G) electric machines (EMs) attached to the low-pressure spool (LPS) of the GTF, arranged as four separate rotor/stator pairs each with four electrically isolated 3-phase alternating current (AC) windings, and each controlled by a separate main generator controller (MGC) inverter/converter unit. Each winding provides power to one EE, which is driven by a pair of electric-engine motors (EEMs) controlled by matching electric-engine motor controllers (EEMC). Rechargeable (secondary) batteries (SBs) are connected to the direct current (DC) bus of each string through a DC/DC converter to assist in stabilizing the bus voltages and to augment the system as needed during periods of high electrical power consumption. The combination of M/G winding, EE, controllers, battery, DC bus, and supporting electrical hardware is referred to as an "electric engine string" and is numbered with its companion EE. All of the EM components are based on a NASA reference design of a 1.4 MW partially superconducting High Efficiency Megawatt Motor (HEMM) [17, 21, 22, 23, 24]. The transient operation of the GTF is improved through the use of a control strategy called Turbine Electrified Energy Management (TEEM) [25]. To enable TEEM, a set of four smaller M/Gs are connected to the high-pressure spool (HPS). These HPS M/Gs are connected to EE strings 05, 08, 11, and 12, and are each controlled by a turbine converter controller (TCC). Due to the use of a single fuel burning engine, backup power is required in the case of a GTF failure. This backup is in the form of large single-use (primary) batteries (PBs) that can be switched in to provide emergency power to the EEs for a limited period, allowing the aircraft to divert to a suitable airport [11]. Figure 3 shows a complete EPS diagram for a single EE string. In general, electrical power is generated by the LPS M/G and sent to the DC bus through the MGC. During steady-state operation, this power is consumed by the EEMs. Whenever there is a mismatch between the power consumed and the power generated, such as during throttle or DEP transients, the DC bus voltage will sag or rise. The DC-DC converter will work to support the bus voltage by charging or discharging the SB. This power can also be used to augment the EE thrust to "boost" the propulsion system. This boost capability is used to reduce the peak thrust and power requirements from the GTF by augmenting the EEs at points such as top of climb (ToC) [16]. This capability can improve engine efficiency by reducing the required core size [26]. Additional detail on the turbomachinery and EPS models is presented in Section IV.

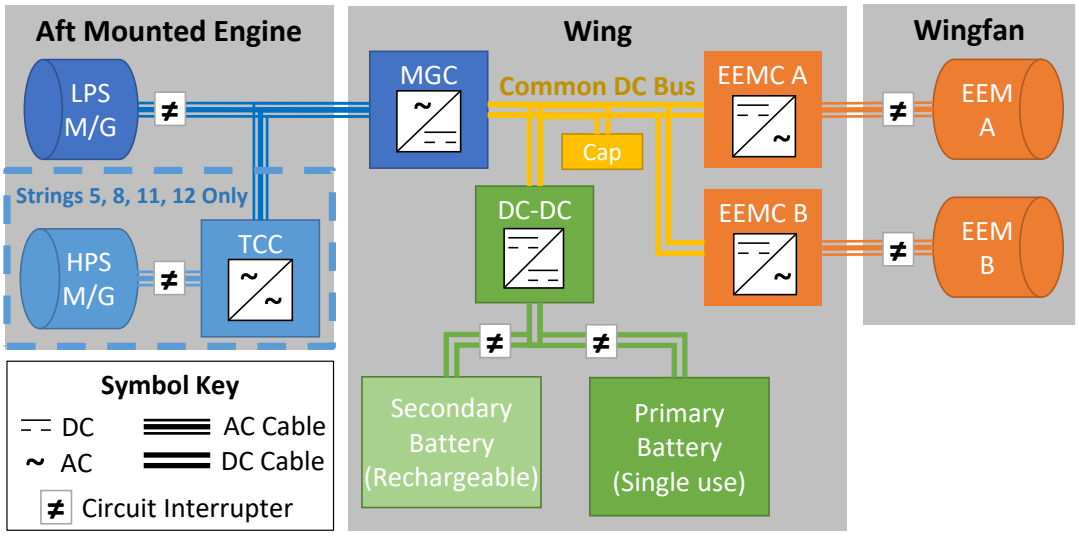

Figure 3. Detailed EPS component diagram of a single SUSAN electric engine string. The EPS consists of all of the electro-mechanical components (Batteries, EMs, inverter/converter units, cables, etc.) in the PPS.

IV. Power/Propulsion Model Updates

The dynamic model of the SUSAN PPS is built in the MATLAB/Simulink® environment using the Toolbox for the Modeling and Analysis of Thermodynamic Systems (T-MATS) [27] and the Electrical Modeling and Thermal Analysis Toolbox (EMTAT) [28]. Both T-MATS and EMTAT were developed by NASA as open-source utilities for dynamic modeling of aero-propulsion and EAP systems. The aft-mounted GTF and wing propulsors [20] are modeled in T-MATS based on an original cycle design created using the Numerical Propulsion System Simulation (NPSS), for which requirements were derived from the SUSAN trade space exploration [15, 20]. The EPS and electro-mechanical actuators are modeled using EMTAT and are incorporated into the Simulink T-MATS model. The controllers for the PPS are also designed and implemented in Simulink, and will be discussed in more detail in Section V. The rest of this section will discuss the dynamic PPS model in more detail, with a focus on the changes implemented to the architecture presented in [16].

A. T-MATS Model and Architecture Updates

The SUSAN PPS propulsion model is a dynamic, non-linear aero-thermal full-envelope model of the GTF and the 16 EEs, built using T-MATS. The SUSAN GTF is similar to an existing NASA reference design for an N+3 commercial engine: the Advanced Geared Turbofan – 30,000 lbf or AGTF30 [16, 29, 30]. The PPS consists of a two-spool geared turbofan engine with a variable bleed valve (VBV), variable area fan nozzle (VAFN), and M/Gs integrated on the LPS and HPS. The aero-thermal model is zero-dimensional and quasi-steady-state (it assumes the mass flow rate, W, through the engine is constant at a given timestep, and does not account for volume dynamics). It uses component performance maps to determine the behavior of the turbomachinery at a given operating point, with a focus on accurately representing the engine shaft dynamics. Transient thermal effects such as heat soak and detailed aerodynamic effects such as BLI are not considered. The T-MATS model uses a fixed timestep of 15ms, which is inherited by the rest of the PPS model.

The SUSAN wingfans are contra-rotating ducted fans with VAFNs arranged in two arrays of eight, one mounted under each wing in a mail-slot configuration. While SUSAN PPS concept has two motors (EEM A and B) in each EE, each driving a one stage of the contra-rotating fan, the T-MATS model captures the performance of both fan stages in a single performance map. As a result, a simplified single shaft model is used with one EEMC and EEM.

Only minor changes were made to the T-MATS model discussed in [16]. In order to enable greater levels of electrical power extraction from the LPS, the high-pressure compressor (HPC) performance map was extrapolated to allow for higher core speeds. The gearbox parameters for the GTF and EE were also updated to assume a fixed, 99% mechanical efficiency. In addition to the changes to the system model, changes were made to the Simulink model architecture and library structure to make the model compatible with the Simulink Coder and allow the model to run in real-time, enabling future applications. These applications are discussed in Section VII.

B. Electrical Power System (EPS) Model Updates

The SUSAN EPS model is built using the EMTAT PowerFlow blockset. The PowerFlow blocks are intended to capture the performance of the EPS on the timescale of turbomachinery shaft dynamics, and use efficiency tables to calculate the voltage, current, and power losses for each component. High frequency electrical dynamics are neglected. Changes made to the model since [16, 17] include updating the battery model, the inclusion of a DC bus capacitor designed to stiffen the bus voltage response, and updated electrical component efficiencies.

The SUSAN primary and secondary batteries are modeled as Li-ion cell packs with a nominal pack voltage of 2000 V. The SBs each have a capacity of 16.1 Ah, a C-rate of 4C, and are sized to provide 125 kW for 5 minutes to support the boost capability. The single-use emergency PBs have a capacity of 312.8 Ah at 2C and are sized to provide 2MW of power for 30 minutes in the case of an engine failure [11]. The underlying battery model is based on the Simulink Simscape Electrical Generic Battery model [31] and is configured to work with the PowerFlow blockset. The battery discharge curve for the SB is shown in Fig. 4. It should be emphasized that this is a nominal model used for control design in the dynamic PPS model only and does not represent results of a detailed battery analysis.

The "Cap" shown on the common DC bus in Fig. 3 represents a set amount of capacitance built into the DC bus. This capacitance stiffens the voltage response in order to reduce fluctuations seen by the SB (preventing rapid switching between charging and discharging). For the SUSAN PPS T-MATS/EMTAT model, the capacitance was set such that the bus time constant, τ, was significantly greater than the model timestep of 15ms, in order to allow the bus voltage dynamics to be captured by the model. The DC bus is modeled as an RC circuit with an equivalent series resistance of R = 0.01 ohms and a capacitance of C = 50 farads, resulting in a τ of 0.5s (τ = RC).

The component efficiencies for the M/Gs and inverter/converter controllers are assumed based on an analysis of the HEMM and its converter [23]. The efficiency maps created for the reference EMTAT HEMM model are shown in Figure 5. For each component, the efficiency maps were scaled based on the power requirements. For example, to create the MGC EMTAT block, the inverter efficiency map shown in Fig. 5 was scaled so that the peak efficiency condition occurred at 2000 V and 961 A, which is the maximum power handled by the MGC under normal operation. All of the inverter/converter control units (the MGC, the EEMC, and the TCC) as well as the DC-DC converter are assumed to have a peak efficiency of 98%. All of the EMs (the LPS and HPS M/Gs, and the EEM) have a peak efficiency of 98.5%. At the peak power condition, which corresponds to the rolling takeoff point (0ft, 0.3 MN), the EEs consume a total of 18.46 MW of electrical power. The power required by the propulsion system lapses with altitude.

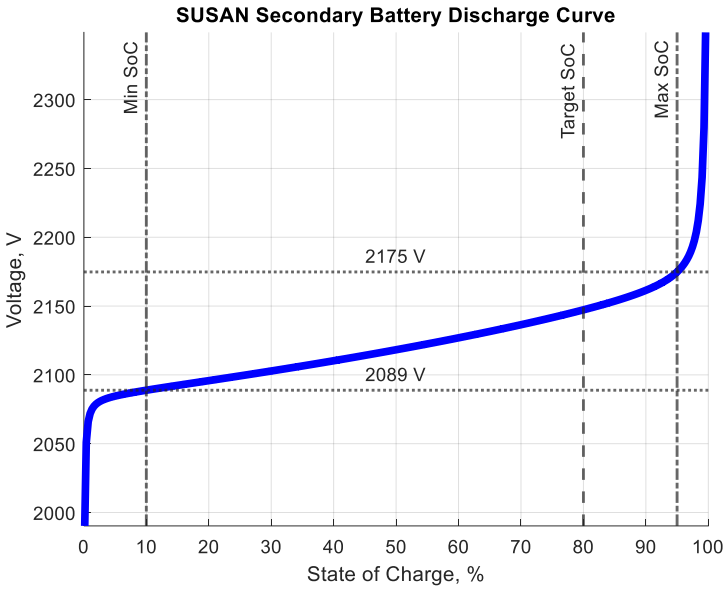

Figure 4. SUSAN nominal SB discharge curve. Minimum and maximum State of Charge (SoC) represent the limits of the linear region used by the system during normal operation.

The TCC is a special component that controls the HPS M/G, which is used primarily to implement TEEM in addition to a small amount of power extraction. The TCC is not connected to the DC bus to allow for a single AC transmission cable to be used for connecting the M/Gs in the tail with the rest of the EPS located in the wings. This means that the TCC is connected in series with the MGC, and must draw AC power from the LP M/G cable and use it to drive the HP M/G. In the EMTAT model, the TCC is represented as two AC/DC converters, however the efficiency is of both converters together assumed to be the same as that of the MGC. Analysis of this arrangement is part of the ongoing SUSAN trade studies. More detailed discussion of the SUSAN EPS hardware development can be found in [17, 24].

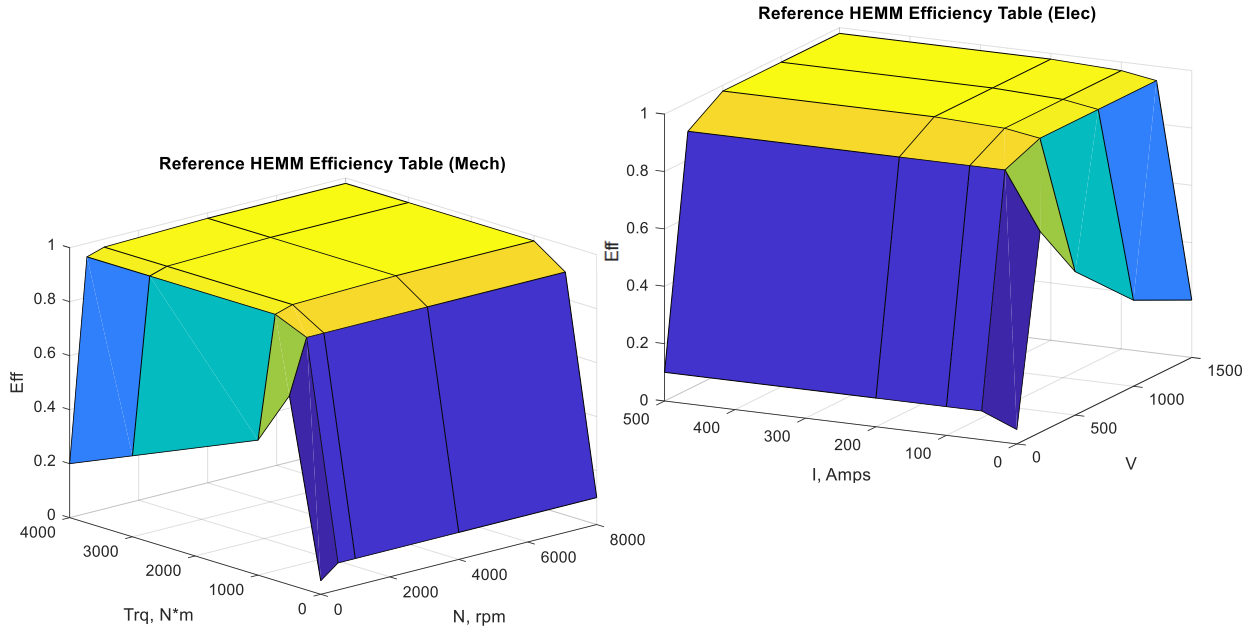

Figure 5. Efficiency maps for reference HEMM motor (left) and inverter (right).

V. Control System Architecture Updates

The changes to the SUSAN PPS control architecture since [16] reflect the updates to the PPS model and expand the capabilities of the dynamic system while improving the system stability. The updates include revised control gains for the EEM and SB SoC controllers, a new strategy for controlling electrical power extraction from the GTF, modifications to the GTF controller to allow increased variability in power extraction, and additional control limiters to protect the GTF and SBs from EM transients. Additionally, the way the PPS receives commands from the pilot or the SUSAN flight control system (FCS) has also been changed to allow for a greater degree of control over the wingfans. A diagram of the updated architecture is shown in Fig. 6. The diagram is intended to illustrate the various interacting control loops and feedback mechanisms and is not an exhaustive list of all of the component interactions within the system. The PPS control architecture is designed with robustness in mind and makes extensive use of gain-scheduled proportional-integral (GS-PI) control loops with integral windup protection (IWP) terms. The general time-domain form for these controllers is shown in Eq. 1:

$$u(t) = K_p e(t) + \int K_i \left(e(t) - K_{iwp}(u(t-1) - u^*(t-1)) \right) dt \tag{1}$$

Here K_i, K_p, and K_{iwp} can be determined via lookup tables. The terms $u(t)$ and $u^*(t)$ represent the ideal and actual controller outputs respectively (ideal being the command from the controller, and actual being the system command accounting for applied limit logic and controller saturation). The $K_{iwp}(u(t-1) - u^*(t-1))$ term will reduce the command from the PI controller over time if the actuator limits have been reached. It is noted that the PPS control architecture is designed to maintain the system within safe operating limits under realistic flight conditions. The control system is designed to be fault tolerant but is not explicitly designed to account for subsystem failures. The system health and fault management of the SUSAN PPS is actively being studied [32].

A. SUSAN PPS Control Architecture Concept of Operations Diagram

The concept of operations for the SUSAN PPS control system, shown in the diagram in Fig. 6, is as follows. The GTF and EEs receive throttle commands from the FCS, shown in Fig. 6 in purple. The throttle commands are converted to corrected shaft speed[1] setpoints (SPs) for each EE and the GTF, whose control loops are shown in blue. The GTF primarily uses a GS-PI loop with IWP to adjust the fuel flow rate, W_f, to control the corrected fan speed, N_{1c}. The EE controllers are also GS-PI loops with IWP, and use the EEM torques to control the corrected wingfan speed, N_{WFc}. The VAFN and VBV actuators for the GTF and EEs are scheduled. The response time of the GTF is limited by the gas path dynamics and ranges from 5 seconds at sea level to 20 seconds at 50,000 ft, while the EEs have a response time of 2 seconds across all flight conditions. During steady-state operation, the GTF M/G electric power extraction is scheduled based on the inlet conditions (*Alt*, *MN*) and N_{1c} to match the nominal power demand from the EEs. However, when there is a mismatch in the power required and the power generated, such as during throttle transients where TEEM is used, DEP maneuvers, or boost, the DC bus voltage will either fall or rise from the 2000V SP. In this case, the DC-DC converter supports the bus voltage, charging or discharging the SB as required. This process uses a regular proportional-integral (PI) loop to maintain the voltage SP and is shown in yellow. The voltage control loop is much faster than the GTF and EE controllers and is tuned to the DC bus time constant, τ = 0.5s. The SB SoC is maintained through another PI loop with IWP, which uses the LP and HP M/Gs to alter the net GTE power extraction to maintain a constant 80% SoC. This controller is always active, however the gains are selected to make it much weaker and slower than the rest of the system control loops (time constant of approximately four minutes) to ensure it does not interfere with normal system dynamics. The SB SoC controller also erases any steady state error between the GTF power supplied and EE power demanded. The purpose of the SB is to decouple the EEs from the GTF, allowing them to respond separately to commands from the FCS. The TEEM controller is only active for short periods during aggressive GTF transients, and uses the HP and LP M/Gs to improve the GTF's thrust response and maintain the compressor stall margins (SMs) through another GS-PI control loop [17, 25]. If for any reason the power consumption of the system were to drop the SB SoC below 10% (the bottom of the linear region of the discharge curve in Fig. 4), the bus voltage would sag and the power available to the EEM and GTF M/Gs would be limited until the SB was sufficiently recharged. These control loops and their relative response times are also listed in Table 1.

The commands from the FCS consist of 17 separate throttle commands (received by the PPS as a nondimensional power lever angle (PLA) between 40 and 80), one for each EE and the GTF. Under normal, steady-state operation these throttle settings are all the same in order to maintain the 1/3 – 2/3 thrust split between the GTF and the EEs and

[1]Corrected shaft speeds are used in place of mechanical shaft speeds to account for variations in ambient conditions from standard day [39].

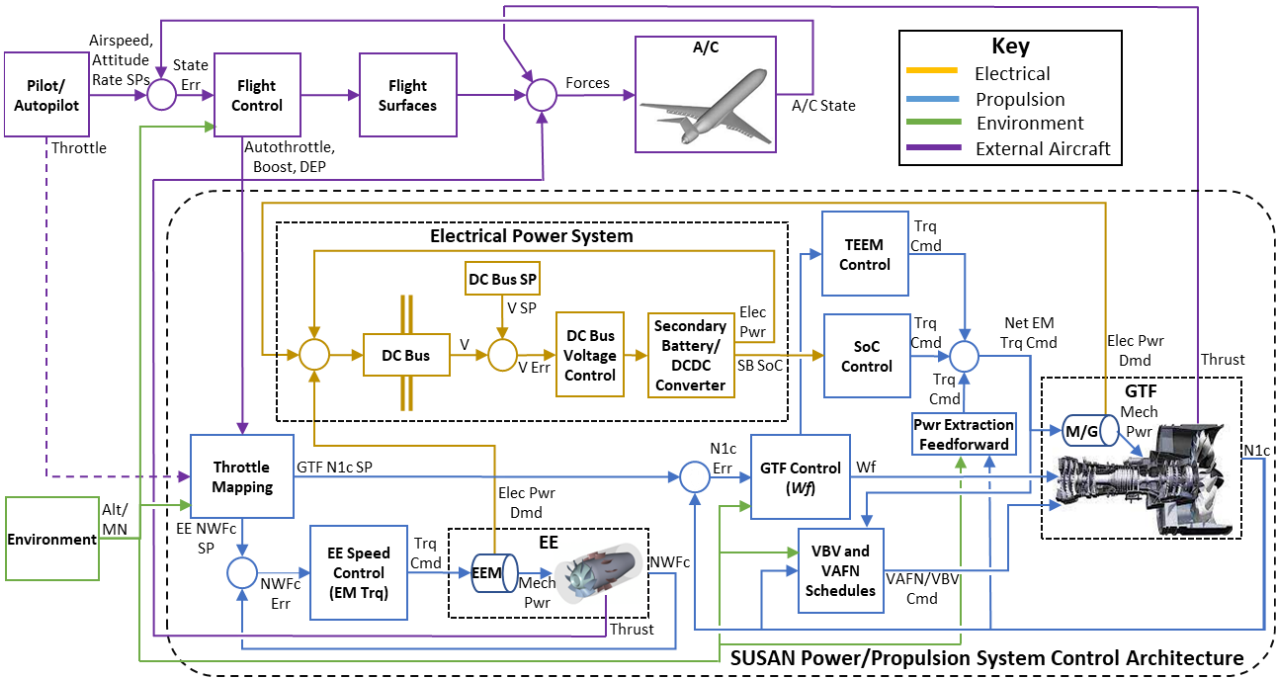

Figure 6. SUSAN PPS Control Architecture. Arrows represent feedback relationships. Repeated components are shown once (Electric Engine (EE), EM and M/G, EPS, etc.). Dual Spool strings not shown explicitly. EE VAFN is scheduled as function of Alt, MN, and wingfan *Nc* and is not shown for simplicity. The PB and switch are also not shown, as are the inverter/converter components. Additional engine sensors used for limit controllers are not shown.

hold the PPS in equilibrium. However, the FCS can adjust the GTF and EE throttles to control the thrust from each engine individually to apply either DEP or boost. The EEs can also respond much more quickly to throttle commands than the GTF and can thus greatly improve the thrust response of the PPS in a case where emergency power is required such as during a rejected landing/go-around. It is noted that the FCS is not considered a part of the PPS model or control system but is included in the diagram as a part of the overall control architecture. The FCS can use a variety of control strategies for determining the thrust allocation during DEP maneuvers, including cascading, pseudo-inverse, and machine-learning (ML) based approaches [19, 33, 34].

The HP M/Gs are only implemented on EE strings 05, 08, 11, and 12 (as shown in Fig. 2), which are referred to as the dual-spool strings. The HP M/Gs are significantly smaller than their LP counterparts and are used for implementing TEEM. This use results in a greater power draw from the SBs attached to the dual-spool strings during throttle transients. Additionally, at higher altitudes and Mach Numbers (MNs) a portion of the total GTF power extraction (up to 12% at MN 0.9, Alt 50,000 ft) comes from the HP M/Gs. This power split is required for maintaining the GTF operability.

While the primary control loops are illustrated in the diagram in Fig. 6, the SUSAN PPS contains a number of conditionally active limit controllers to protect the GTF, EEs, and EPS. The GTF fuel flow controller incorporates several conditionally active limit controllers that it switches between using min-max ladder logic. The EE controller incorporates overspeed protection, and the SoC controller EPS includes limits to protect the low pressure compressor (LPC) pressure ratio (PR) and prevent battery overcharging. The limit controllers are summarized in Table 2.

Table 1. SUSAN PPS Primary Control Loops

Control Loop	Variable	Response Time
GTF Speed Control	W_f	5 – 20 sec
EE Speed Control	EEM Torque	2 sec
TEEM Control	HP and LP M/G Torque	< 5 sec
SB SoC Control	HP and LP M/G Torque	> 240 sec
DC Bus Voltage Control	SB charge/discharge current	< 0.5 sec

Table 2. SUSAN PPS Limit and Transient Controllers

PPS System	Controller/Limit	Summary/Purpose
GTF	T_3 Max	Limits the HPC discharge temperature
	T_4 Max	Limits the high-pressure turbine (HPT) inlet temperature
	N_2 Max	Prevents LPS overspeed
	N_3 Max	Prevents HPS overspeed
	P_{s3} Min/Max	Maintains the HPC discharge pressure between the maximum and minimum values
	W_f Min	Prevents combustor blowout by maintaining a minimum fuel flow
	Accel/Decel (W_f/P_{s3})	Uses W_f/P_{s3} ratio unit (RU) based W_f schedules to protect engine operability during aggressive transients
	TEEM	Uses LP and HP M/Gs to assist GTE W_f controller when the error in the active control variable is above a certain threshold
EE	N_{WF} Max	Prevents EE overspeed
EPS	P_{25}/P_2 Min	Protects LPC pressure ratio under varying power extraction
	Max charge power	Limits SB SoC controller electrical power extraction to protect GTF
	SB overcharge protection	Prevents SB overcharging through a washout term that limits power extraction if SoC approaches maximum (95%)

B. Discussion and Observations

This section will also discuss some observations made during the process of updating and validating the updated control system, in comparison with the previous iteration in [16]. The overall objective while developing the SUSAN PPS control architecture was to build a flexible, full-envelope controller for a highly integrated MW-scale series/parallel partial hybrid-electric powertrain. The control concept uses a series of overlapping PI control loops with various complimentary goals. The overlapping controllers are designed with different time constants to prevent them from interfering with each other. To demonstrate the robustness of the controller architecture, the system was tested with an aggressive throttle profile at various fixed points within the SUSAN PPS flight envelope, illustrated in Fig. 7. The controller was able to maintain the thrust response, DC bus voltage, and SB SoCs of the system across all the test cases while respecting all of the imposed turbomachinery and electrical hardware limits.

The biggest set of changes was made to the EE controllers in order to allow them to be commanded independently of the GTF. Previously the EE N_{WFc} SP tracked the GTF N_{1c} SP and DEP/Boost was handled by commanding a delta N_{WFc} SP, which limited the control bandwidth. Independent throttle control simplifies the PPS integration with the FCS and allows the FCS to leverage the higher faster response time of the EEMs as compared to the GTF. In order to allow the EEs to track the faster moving setpoints, the control gains had to be modified. Because the EE N_{WFc} SPs are no longer based on the GTF SPs, revisions were also made to the power extraction and SoC controllers. The

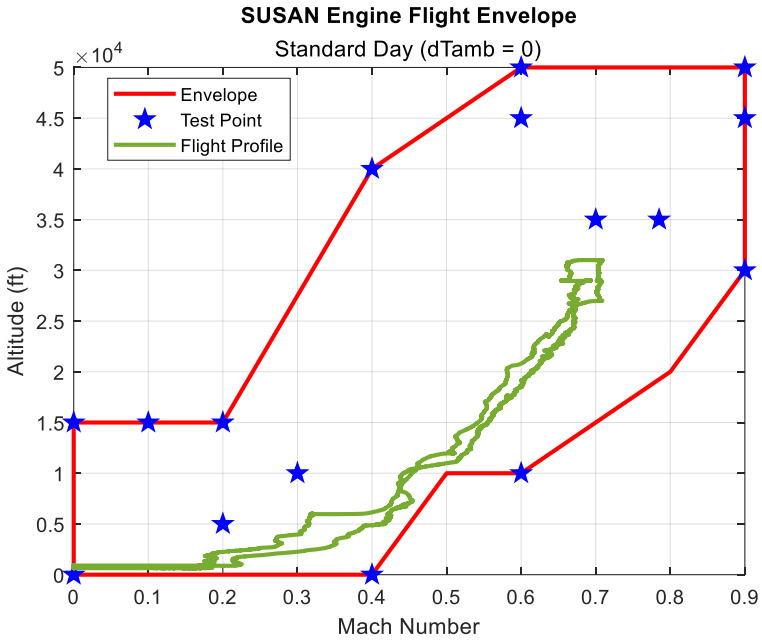

Figure 7. SUSAN PPS flight envelope. Test points are operating points used to validate the control design. Flight profile [36] represents a 90-minute flight used as another test of the system.

base level of power extraction is now scheduled based on the GTF shaft speeds instead of being determined directly by the EE demand. In order to support the larger SBs needed to support the boost capability, the SB SoC controller needed to be able to adjust power extraction from the GTF. In order to protect the GTF operability under varying levels of power extraction, two separate limits are used. The first limit saturates SB SoC controller power command based on the altitude and throttle setting, and the second prevents the power extraction from increasing when the GTF T_4, Max N_3, or P_{s3} Min limiters are active or if the LPC PR drops below a certain threshold. The increased variability in power extraction also required that the GTF VBV schedule be modified to include a dependency on the level of power extraction in order to maintain the LPC PR. The HPC component map was also extended. The effects of varying power extraction on a hybrid turbofan are discussed further in [35].

VI. Model Results and Validation

Results from the dynamic SUSAN PPS model are shown in Figs. 8, 9, and 11. Three different scenarios are shown to illustrate different capabilities of the system and controller. Boost and DEP are demonstrated at cruise to show how the system responds to the independent control of the wing fans. Results for a throttle burst/chop (rapid transient from idle to full power and back) at sea-level-static (SLS) conditions are shown to illustrate the TEEM controller and the

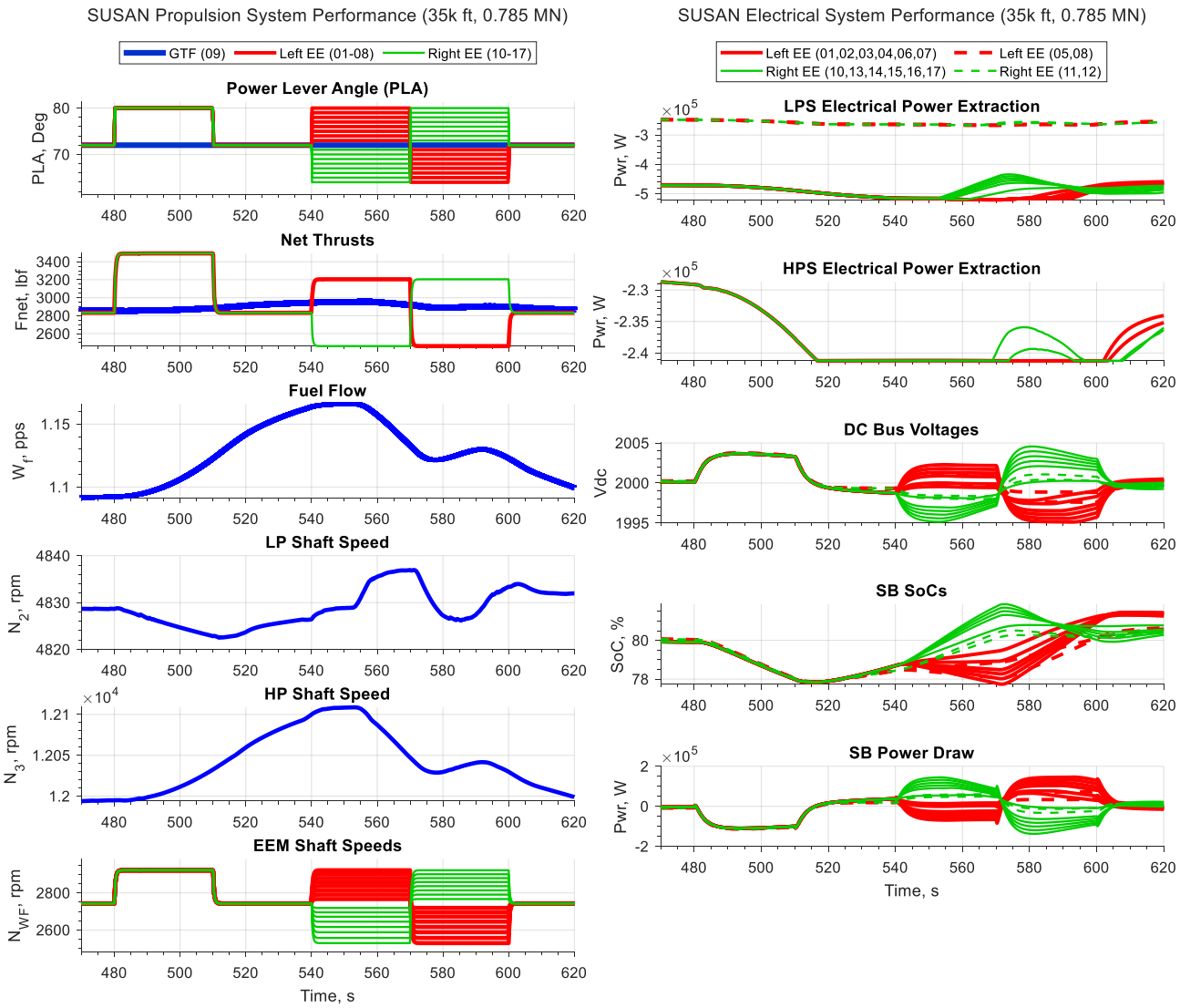

Figure 8. PPS and EPS data for a boost followed by a nominal DEP maneuver at cruise conditions (Alt = 35,000 ft, MN = 0.785). Power generation sign convention is negative for power extraction, positive for power injection.

comparative response times of the system. Finally, results from a simulated, 90-minute flight are shown to demonstrate the successful operation of the controller under realistic operating conditions.

Figure 8 shows the response of the system to a 30 second throttle boost, followed by a 60 second nominal DEP command. The GTF throttle command is held constant at 72 degrees. It can be seen that the systems respond as expected, and the controller maintains the GTF shaft speed N_{1c} within a range of 10 rpm while varying the EE speeds in response to the throttle (PLA) commands. The SB is drained during the boost period, but the SoC begins to recover when the system returns to steady state. The small fluctuations in GTF shaft speed come from the changing levels of power extraction, as can be seen in the plots LPS and HPS power extraction. These plots also illustrate the power extraction split between the LPS and HPS required at higher altitudes. The difference in behavior between the EE strings with two M/Gs (05, 08, 11, and 12) and those with only one can be seen in the power extraction results as well. The DEP command given in this example is a simple linear cascade used to illustrate the system behavior and doesn't represent a specific command from the FCS.

Figure 9 shows the response of the SUSAN PPS to a throttle burst/chop maneuver at SLS. As in the previous example, the system behaves as expected. The difference in response times between the GTF and the EEs can be seen in the thrust response plot on the left. This example also demonstrates the TEEM control being activated during the acceleration and deceleration, as can be seen the power extraction plots. At sea level, no power is extracted from the

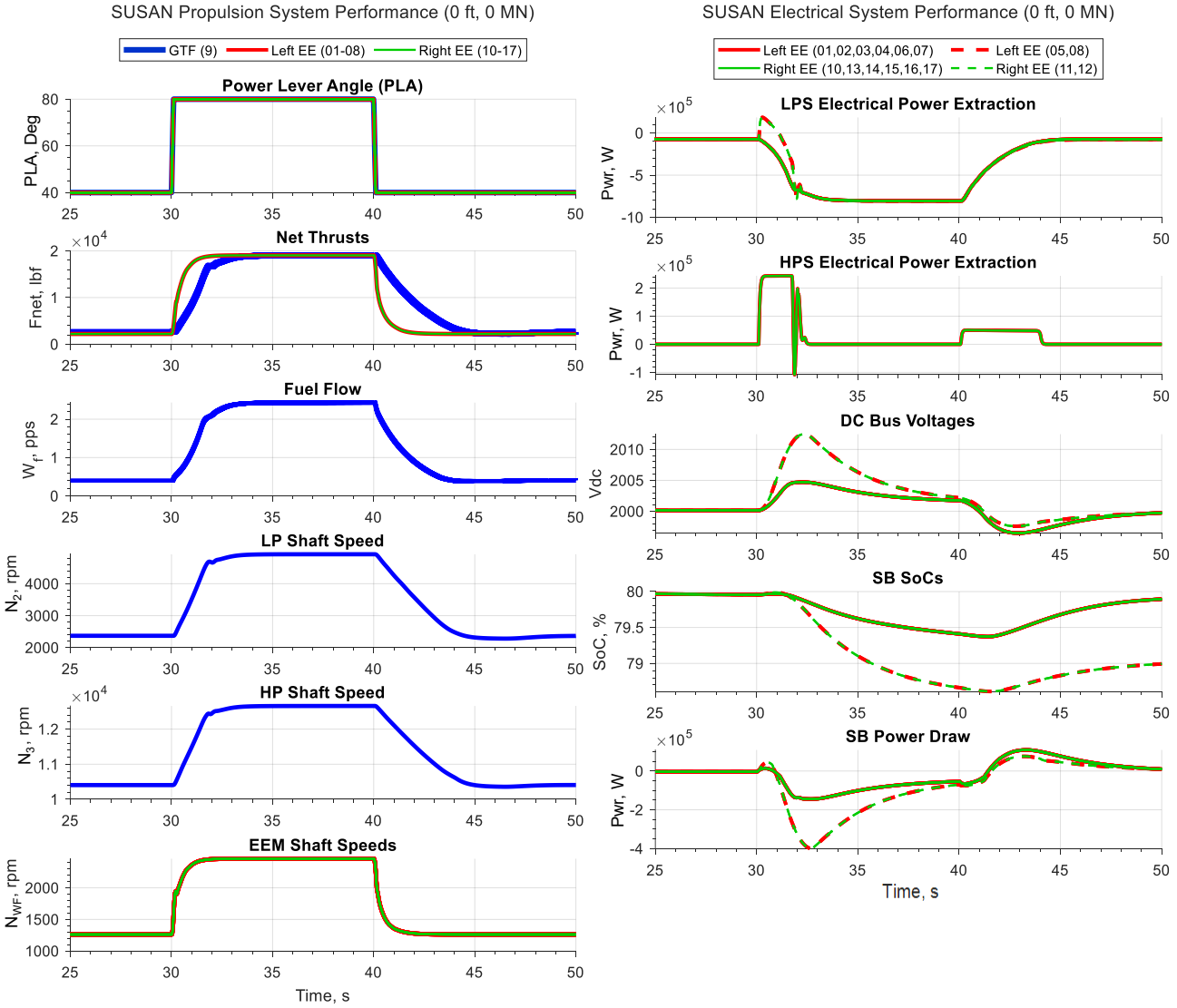

Figure 9. PPS and EPS data for burst/chop maneuver at SLS conditions (Alt = 0 ft, MN = 0). The difference in the GTF and EE thrust response times can be seen in the Net Thrusts plot in the left column.

HPS so TEEM is the only use of the HP M/Gs. The LP M/G power extraction is the sum of the scheduled power extraction, SB SoC controller, and TEEM controller power commands. It is noted that the SB SoCs for the EE strings with two M/Gs drop nearly 1% further than the SBs with 1 M/G during the TEEM acceleration. Optimally sizing the batteries for the different EE strings is a topic that should be investigated as the SUSAN concept continues to mature.

Figures 10 and 11 show the inputs and the system behavior for a simulated, 90-minute flight profile (not including pre- and post-flight taxi). The throttle, altitude, and MN inputs are shown in Fig. 10. The altitude, MN, and original throttle profiles are based on de-identified recorded flight data taken from the NASA DASHlink website [36]. The throttle profile was then modified to add simulated boost and DEP events at relevant points such as cruise and ToC. These inclusions are nominal and are not based on any specific SUSAN flight, but are used to demonstrate the response of the PPS to these inputs over the simulated mission. The propulsion system and EPS performance are shown in Fig. 11. Again, the control system behaves as intended and successfully manages the thrust response, SB SoCs, and DC bus voltages for the duration of the flight. The extra power drain from the 4 EE strings with two M/Gs is even more pronounced during the climb phase, causing the SoC to drop below 30%, however it is able to recover during the cruise phase. Observations from the results depicted here will be accounted for as the PPS model and controller continue to mature alongside the rest of the SUSAN concept.

VII. Applications and Planned Testing

In addition to being a demonstration of a control architecture for a tightly integrated series/parallel partial hybrid electric powertrain, the dynamic SUSAN PPS model and control architecture presented in this paper were developed with the intention of using them for a number of upcoming studies. The PPS model and controller are intended to be integrated into an updated full-scale model of the SUSAN Electrofan aircraft including an aerodynamic model and FCS. This model can be used for sizing and optimization studies to provide more detailed requirements for capabilities such as boost, form the basis for ongoing research into EAP system health management and fault accommodation, and to further explore the SUSAN trade space in an effort to mature the concept. Flight controls and instrumentation have been added to the full-scale SUSAN model for use in piloted flight simulator studies, similar to previous work performed at GRC using earlier versions of the SUSAN model [37] as well as other EAP concepts [12]. The updated PPS model can also be used for hardware-in-the-loop controls testing in the Hybrid Propulsion Emulation Rig

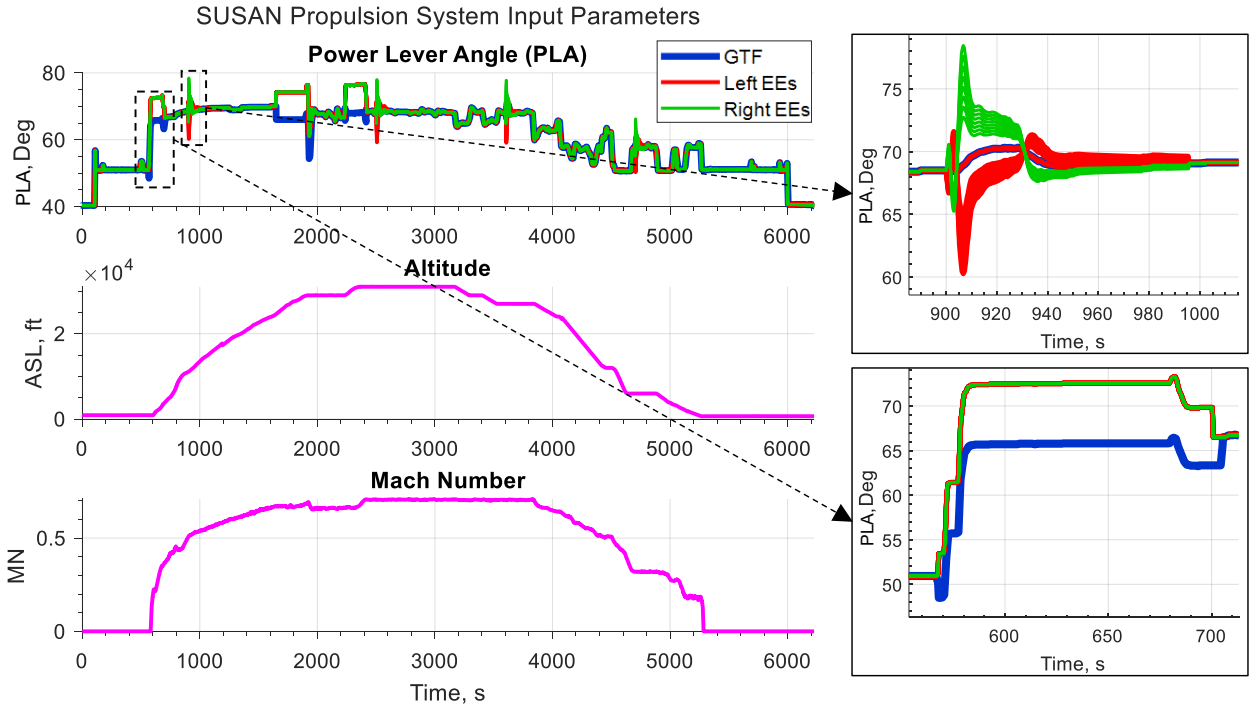

Figure 10. PPS Model inputs for a simulated 90-minute flight profile [36]. Baseline throttle , MN and Alt inputs come from recorded flight data. Throttle (PLA) profile has been modified to incorporate DEP and boost inputs (examples in inset details). Three periods of boost and four DEP maneuvers are included.

(HyPER) facility at GRC [38], in order to both further validate the control concept and expand the capabilities of the HyPER lab. Finally, there is room for additional optimization of the control system, and the underlying T-MATS/EMTAT model can be used to support further control design studies using alternate approaches.

VIII. Conclusions

An updated control architecture developed for the Subsonic Single Aft eNgine (SUSAN) Electrofan concept aircraft power/propulsion system (PPS) was developed. The control architecture is intended to be robust, and leverages overlapping proportional-integral control loops to achieve the objectives of the PPS. Results from the dynamic PPS model demonstrate that the control architecture is capable of responding to simulated commands from the SUSAN flight control system (FCS) and delivering the required thrust response while maintaining stability and managing the energy levels of the PPS system. These results validate the control design approach and demonstrate that PI control is sufficient for complex and tightly integrated EAP systems. The dynamic PPS model is intended to be used for a number of planned studies and tests, the results of which will be fed back into the SUSAN trade space analysis. Future revisions of the SUSAN concept will also motivate future updates to this PPS model and controller.

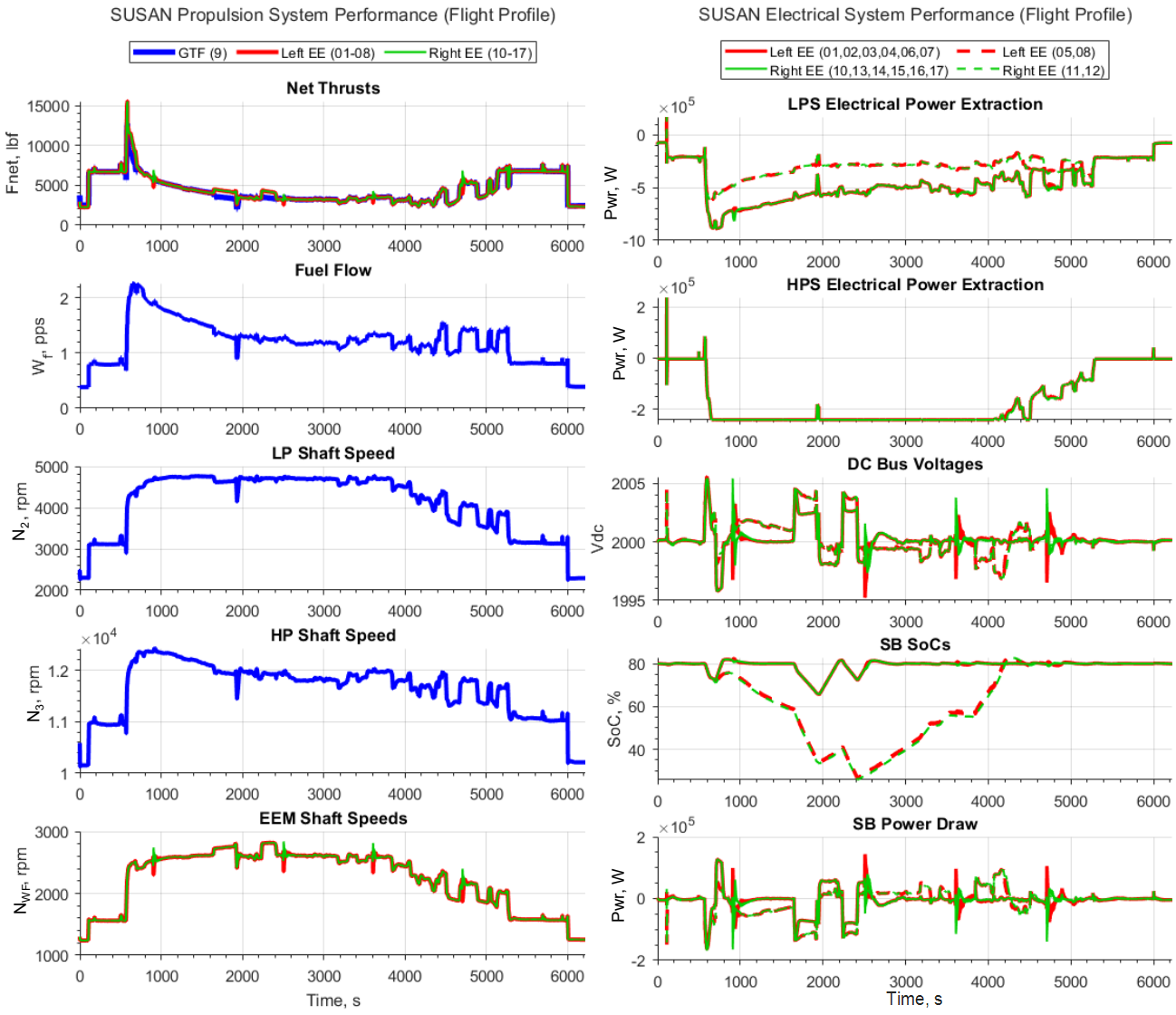

Figure 11. PPS and EPS data for a simulated 90 minute full-flight profile with boost and DEP. The additional drain on the SBs for EEs 05, 08, 11, and 12 can be seen in the SB SoC plot. The changing power extraction split between the HP and LP M/Gs can also be seen.

Acknowledgments

The authors acknowledge the Transformational Tools and Technologies (TTT) and Convergent Aeronautics Solutions (CAS) projects of NASA's Transformative Aeronautics Concepts Program (TACP) for funding this research, as well as the contributions and advice of Timothy P. Dever, Santino J. Bianco, and Ralph H. Jansen, all of the NASA Glenn Research Center.

References

[1] D. S. Lee, D. W. Fahey, A. Skowron, M. R. Allen and U. Burkhardt, "The contribution of global aviation to anthropogenic climate forcing for 2000 to 2018," *Atmospheric Environment*, vol. 244, no. ISSN 1352-2310, 2021.

[2] G. B. Gratton, P. D. Williams, A. Padhra and S. Rapsomani, "Reviewing the impacts of climate change on air transport operations," *The Aeronautical Journal*, vol. 126, no. 1295, p. pp. 209–221, 2022.

[3] T. Ryley, S. Baumeister and L. Coulter, "Climate change influences on aviation: A literature review," *Transport Policy*, vol. 92, no. 0967-070X, pp. 55-64, 2020.

[4] National Aeronautics and Space Administration, "Sustainable Flight National Partnership," 2022. [Online]. Available: https://www.nasa.gov/sfnp/. [Accessed 3 2023].

[5] National, Academies of Sciences, Engineering, and Medicine, et al., "Commercial Aircraft Propulsion and Energy Systems Research : Reducing Global Carbon Emissions," National Academies Press, 2016, Washington, DC, 2016.

[6] National Aeronautics and Space Administration, "NASA Aeronautics Strategic Implementation Plan," NASA Aeronautics Research Mission Directorate, Washington D.C., 2019.

[7] United States Federal Aviation Administration, "United States 2021 Aviation Climate Action Plan," FAA, 2021.

[8] E. Piñero, "Electric vertical takeoff and landing aircraft dominate powered-lift community focus," Aerospace America, December 2022. [Online]. Available: https://aerospaceamerica.aiaa.org/year-in-review/electric-vertical-takeoff-and-landing-aircraft-dominate-powered-lift-community-focus/. [Accessed 9 March 2023].

[9] R. H. Jansen, C. Bowman, A. Jankovsky, R. Dyson and J. Felder, "Overview of NASA Electrified Aircraft Propulsion Research For Large Subsonic Transports," in *AIAA Propulsion and Energy Forum*, Atlanta, GA, 2017.

[10] R. W. Dyson, "NASA Electric Aircraft Test bed (NEAT) Development Plan - Design, Fabrication, Installation," NASA/TM—2016-219085, Cleveland, OH, 2016.

[11] C. L. Denham and R. H. Jansen, "Initial Regulatory and Certification Approach for the SUSAN Electrofan Concept," in *AIAA SciTech Forum*, San Diego, CA, 2021.

[12] J. S. Litt, J. J. Sachs-Wetstone, D. L. Simon, T. S. Sowers, A. K. Owen and M. E. Bell, "Flight Simulator Demonstration and Certification Implications of Powertrain Failure Mitigation in a Partial Turboelectric Aircraft," in *AIAA/IEEE Aviation/Electrified Aircraft Technology Symposium (EATS)*, San Diego, CA, 2023.

[13] S. Adibhatla, J. Ding, S. Garg, S. Griffith, K. Karnofski, N. Payne, D. Simon and B. Wood, "Propulsion Control Technology Development Needs to Address NASA Aeronautics Research Mission Goals for Thrusts 3a and 4," in *AIAA Propulsion and Energy Forum Joint Propulsion Conference*, Cincinnati, Ohio, 2018.

[14] D. L. Simon, "System-Level Control Concepts for Electrified Aircraft Propulsion Systems," NASA/TM-20210026284, Cleveland, Ohio, January 2022.

[15] R. H. Jansen, C. C. Kiris, T. Chau, G. K. W. Kenway, L. G. Machado and J. C. Duensing, "Subsonic Single Aft Engine (SUSAN) Transport Aircraft Concept and Trade Space Exploration," in *AIAA SciTech Forum*, San Diego, CA, 2022.

[16] J. S. Litt, J. L. Kratz, J. S. Bianco, J. J. Sachs-Wetstone, P. T. Dever and H. E. Buescher, "Control Architecture for a Concept Aircraft With a Series/Parallel Partial Hybrid Powertrain and Distributed Electric Propulsion," in *AIAA SciTech Forum*, National Harbor, MD, 2023.

[17] J. W. Chapman, J. L. Kratz, P. T. Dever, A. Mirhashemi, E. J. Stalcup, W. R. Sixel, A. A. Woodworth, R. H. Jansen and N. Heersema, "Update on SUSAN Concept Vehicle Power and Propulsion System," in *AIAA SciTech Forum*, National Harbor, MD, 2023.

[18] J. M. Haglage, T. P. Dever, R. H. Jansen and M. A. Lewis, "Electrical System Trade Study for SUSAN Electrofan Concept Vehicle," in *AIAA SciTech Forum*, San Diego, CA, 2021.

[19] L. Machado, T. Chau, G. K. Kenway, J. C. Duensing and C. C. Kiris, "Preliminary Assessment of a Distributed Electric Propulsion System for the SUSAN Electrofan," in *AIAA SciTech Forum and Exposition*, National Harbor, MD, 2022.

[20] A. Mirhashemi, J. W. Chapman, C. J. Miller, J. E. Stephens and R. H. Jansen, "Tail-mounted engine Architecture and Design for the Subsonic Single Aft Engine Electrofan Aircraft," in *AIAA SciTech Forum*, San Diego, CA, 2022.

[21] R. H. Jansen, Y. De Jesus-Arce, P. Kascak, R. Dyson and A. Woodworth, "High Efficiency Megawatt Motor Conceptual Design," in *AIAA Propulsion and Energy Forum and Exposition*, Cincinnati, OH, 2018.

[22] R. H. Jansen, P. Kascak, R. Dyson, A. Woodworth, J. Scheidler, A. D. Smith, E. Stalcup, T. Tallerico, Y. D. Jesus-Arce and D. Avanesian, "High Efficiency Megawatt Motor Preliminary Design," in *AIAA/IEEE Electric Aircraft Technologies Symposium (EATS)*, Indianapolis, Indiana, 2019.

[23] M. Granger, A. Anderson, J. M. Maroli, T. Tallerico and J. J. Scheidler, "Combined Analysis of NASA's High Efficiency Megawatt Motor and Its Converter," in *AIAA/IEEE Electric Aircraft Technologies Symposium (EATS)*, Denver, CO, August 2021.

[24] T. Tallerico, A. D. Anderson, J. J. Scheidler and R. H. Jansen, "Concept Design for a 5 MW Partially Superconducting Generator," in *AIAA AVIATION Forum and Exposition*, San Diego, CA, June 2023.

[25] J. Kratz, D. Culley and G. Thomas, "Turbine Electrified Energy Management (TEEM) For Enabling More Efficient Engine Designs," in *Joint Propulsion Conference*, Cincinnati, OH, 2018.

[26] C. L. Bowman, J. L. Felder and T. V. Marien, "Turbo-and Hybrid-Electrified Aircraft PropulsionConceptsfor Commercial Transport," in *AIAA/IEEE Electric Aircraft Technologies Symposium*, Cincinnati, OH, July 2018.

[27] J. Chapman, T. Lavelle, R. May, J. Litt and T.-H. Guo, "Toolbox for the Modeling and Analysis of Thermodynamic Systems (T-MATS) User's Guide," NASA/TM-2014-216638, January 2014.

[28] M. E. Bell and J. S. Litt, "Electrical Modeling and Thermal Analysis Toolbox (EMTAT) User's Guide," NASA/TM 20205008125, October 2020.

[29] J. Chapman and J. S. Litt, "Control Design for an Advanced Geared Turbofan Engine," in *AIAA/ASME/SAE/ASEE Joint Propulsion Conference*, Atlanta, GA, 2017.

[30] S. M. Jones, W. J. Haller and M. T. Tong, "An N+3 Technology Level Reference Propulsion System," NASA/TM—2017-219501, Cleveland, OH, 2017.

[31] The MathWorks, Inc., "Generic Battery Model - Simulink," mathworks.com, [Online]. Available: https://www.mathworks.com/help/sps/powersys/ref/battery.html. [Accessed 28 November 2023].

[32] J. S. Litt, J. J. Sachs-Wetstone, H. E. Buescher, T. S. Sowers, A. K. Owen, K. Wu and J. Tierney, "System Health Management for a Series/Parallel Partial Hybrid Powertrain with Distributed Electric Propulsion," in *Targeted for Publication at the AIAA SciTech Forum*, Orlando, FL, 2024.

[33] A. P. Nicholas C. Ogden, "A Framework for Evaluating Distributed Electric Propulsion on the SUSAN Electrofan Aircraft," NASA/TM–20230009523, July 2023.

[34] K. Wu and J. S. Litt, "Reinforcement Learning Approach to Flight Control Allocation with Distributed Electric Propulsion," NASA/TM-20230014863, Cleveland, OH, November 2023.

[35] J. W. Chapman, "Considering Turbofan Operability in Hybrid Electric Aircraft Propulsion System Design," in *AIAA 2023-2178. AIAA SCITECH 2023 Forum*, National Harbor, MD, January 2023.

[36] B. Matthews and N. Oza, "NASA DASHlink Sample Flight Data," NASA, 29 November 2012. [Online]. Available: https://c3.ndc.nasa.gov/dashlink/projects/85/. [Accessed 2022].

[37] J. S. Litt, T. S. Sowers, H. E. Buescher, J. J. Sachs-Wetstone, N. S. Listgarten and R. H. Jansen, "Implementation Approach for an Electrified Aircraft Concept Vehicle in a Research Flight Simulator," in *AIAA SciTech Forum*, San Diego, CA, January 2022.

[38] H. E. Buescher, D. E. Culley, S. Bianco, J. W. Connolly, A. Dimston, J. Saus, C. Theman, K. R. Hunker, M. J. Garrett, J. M. Haglage, M. A. Horning, Y. C. Cha and N. Purpera, "Hybrid-Electric Aero-Propulsion Controls Testbed: Overview and Capability," in *AIAA SCITECH 2023 Forum*, National Harbor, MD, January 2023.

[39] A. J. Volponi, "GAS TURBINE PARAMETER CORRECTIONS," in *International Gas Turbine & Aeroengine Congress & Exhibition*, Stockholm, Sweden, June 1998.